Full Wave Simulations for Fast Wave Heating and Power Losses in the Scrape-off Layer of Tokamak Plasmas

N. Bertelli[1], E. F. Jaeger[2], J. C. Hosea[1], C. K. Phillips[1], L. Berry[3], P. T. Bonoli[4], S. P. Gerhardt[1], D. Green[3], B. LeBlanc[1], R. J. Perkins[1], C. M. Qin[5], R. I. Pinsker[6], R. Prater[6], P. M. Ryan[3], G. Taylor[1], E. J. Valeo[1], J. R. Wilson[1], J. C. Wright[4] and X. J. Zhang[5]

[1]Princeton Plasma Physics Laboratory, Princeton NJ 08543, USA
[2]XCEL Engineering Inc., Oak Ridge, TN 37830, USA
[3]Oak Ridge National Laboratory, Oak Ridge, TN 37831-6169, USA
[4]Plasma Science and Fusion Center, MIT, Cambridge, MA 02139, USA
[5]Institute of Plasma Physics, Chinese Academy of Sciences, Hefei 230031, Peoples Republic of China
[6]General Atomics, PO Box 85608, San Diego, CA 92186-5608, USA

Corresponding Author: nbertell@pppl.gov

1 Introduction

In fusion experiments, fast wave heating in the ion cyclotron range of frequency (ICRF) has been successfully used to sustain and control the plasma performance. Consequently, ICRF heating will likely play an important role in the ITER experiment [1]. However, many ICRF heating experiments have found regimes in which significant fractions of the coupled RF power does not appear in the core, in some cases as much as 50% or more of the applied power. Experimental studies employing high harmonic fast wave (HHFW) heating on the National Spherical Torus eXperiment (NSTX) [2], a low aspect ratio tokamak, have shown that substantial HHFW power loss (up to 60% of the HHFW power coupled from the antenna) can occur along the open field lines in the scrape-off layer (SOL) when edge densities are high enough that the FWs can propagate close to the antenna. The mechanism behind this loss in the SOL is not yet understood [3]-[7]. This paper examines FW power loss in the SOL by using the numerical full wave simulation code AORSA [8], in which the edge plasma beyond the last closed flux surface (LCFS) is included in the solution domain [9]. A collisional damping parameter is used as a proxy to represent the real, and most likely nonlinear, damping processes [10, 11] in order to predict the effects, and possible causes, of this power loss. This numerical approach is applied to specific NSTX discharges and to "conventional" tokamaks with higher aspect ratios, such as DIII-D and EAST. Furthermore, a prediction for the NSTX Upgrade (NSTX-U)

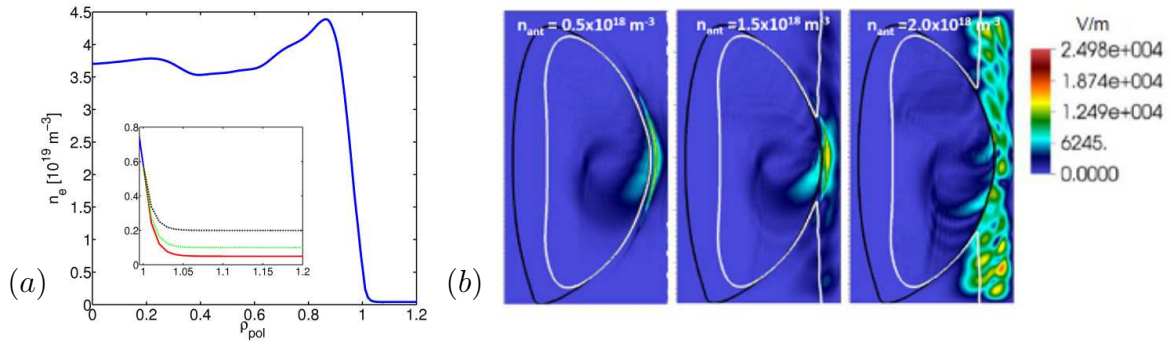

FIG. 1: Fig. (a): Electron density, n_e, as a function of the square root of the normalized poloidal flux, ρ_{pol}, for NSTX shot 130608. The insert figure shows a closer view of the exponential decay of the density profile in the SOL for three different values of the density in front of the antenna: $n_{ant} = 0.5 \times 10^{18}$, 1.0×10^{18}, and 2.0×10^{18} m^{-3}. Fig. (b): Electric field amplitude for different density values in front of the antenna (n_{ant}) (shown in the plots) with toroidal mode numbers $n_\phi = -21$. The white and black curves indicate the FW cut-off layer and the LCFS, respectively.

experiment, that will begin operation next year, is also presented, indicating a favorable condition for the experiment due to a wider evanescent region in edge density.

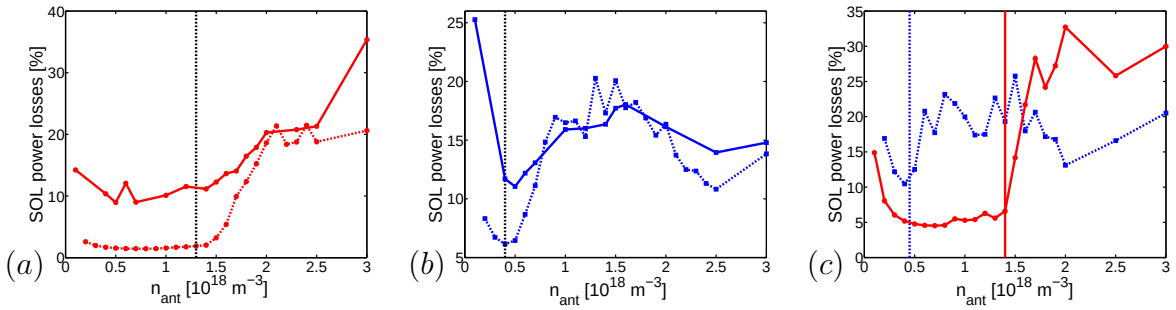

FIG. 2: Figs. (a) and (b): Fraction of power lost to the SOL as a function of the density in front of the antenna, comparing the 3D runs (solid curves) with the dominant mode runs (dashed curves), for $n_\phi = -21$ (a) and $n_\phi = -12$ (b), for NSTX shot 130608. Fig. (c): Fraction of power lost to the SOL as a function of the density in front of the antenna for $n_\phi = -21$ (solid curve) and $n_\phi = -12$ (dashed curve) for NSTX shot 130621. The vertical lines represent the value of the density for which the FW cut-off starts to be "open" in front of the antenna.

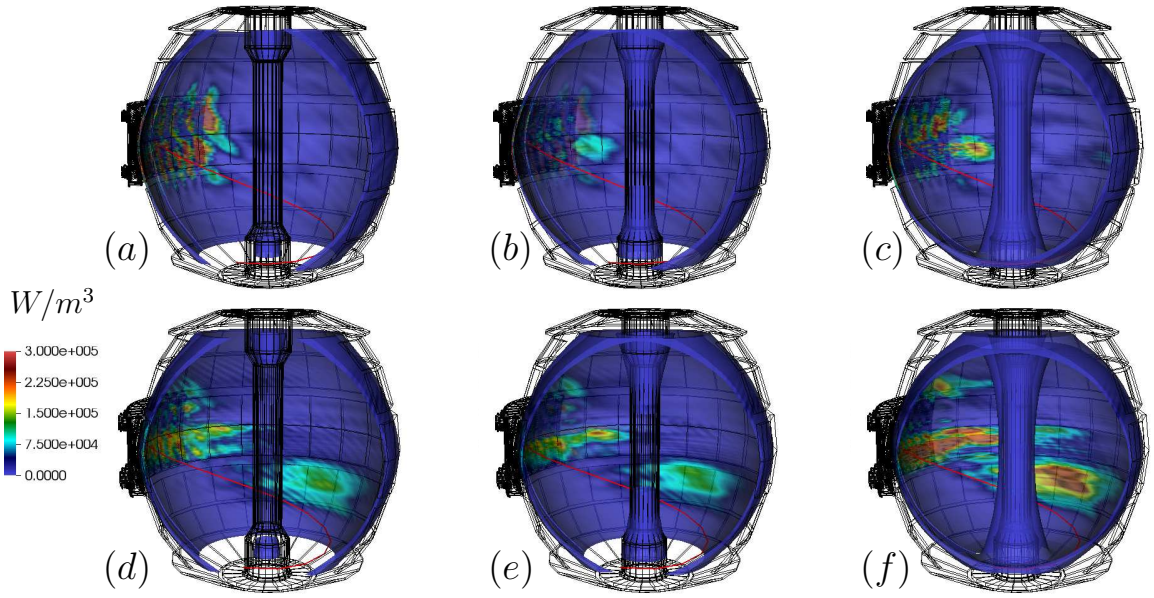

FIG. 3: 3D contour plots of the absorbed power in the SOL for two different value of the density in front of the antenna (assuming $\nu/\omega = 0.01$) for NSTX shot 130608: $n_{\rm ant} = 1.0 \times 10^{18}$ m^{-3} in (a-c) and $n_{\rm ant} = 2.5 \times 10^{18}$ m^{-3} in (d-f). Three different ρ slices are shown: (a) and (d) $\rho = 1.1$ to 1.15 (near the antenna located at $\rho \simeq 1.15$), (b) and (e) $\rho = 1.05$ to 1.1 (mid SOL), and (c) and (f) $\rho = 1$ to 1.05 (near the LCFS). The red curve represents a magnetic field line starting from the antenna and shows the large pitch angle of the magnetic field with respect to the antenna.

2 Numerical Results for NSTX

AORSA is a full wave code that solves the Helmholtz wave equation for a tokamak geometry, including the SOL region beyond the LCFS where the magnetic field lines are open [8, 9]. The density profile adopted in the SOL is given by

$$n_{\rm e} = n_{\rm e,ant} + [n_{\rm e}(\rho = 1) - n_{\rm e,ant}] \exp\left[\frac{\rho - 1}{d_{\rm SOL}}\right], \quad \rho \geq 1 \tag{1}$$

where an exponential decay is prescribed from the LCFS, $n_{e,ant}$ is a minimum density in front of the antenna, ρ is the square root of the normalized poloidal flux, and $d_{\rm SOL}$ is a SOL decay length. $n_{e,ant}$ and $d_{\rm SOL}$ are AORSA's input and they can be modified in order to fit as best as possible the experimental data [9]. Within the LCFS, the density profile is given by the measurements. In Fig. 1(a) the electron density profile as a function of the square root of the poloidal flux is shown and the insert figure shows the exponential density profiles in the SOL for $d_{\rm SOL} = 0.01$ and three different values of $n_{e,ant}$.

Figure 1(b) shows the wave electric field amplitude obtained by the 2D full wave code AORSA for a single (dominant) toroidal mode, $n_\phi = -21$ for NSTX shot 130608 for three different values of the density in front of the antenna ($\rm n_{ant} = 0.5 \times 10^{18}$, 1.5×10^{18}, and

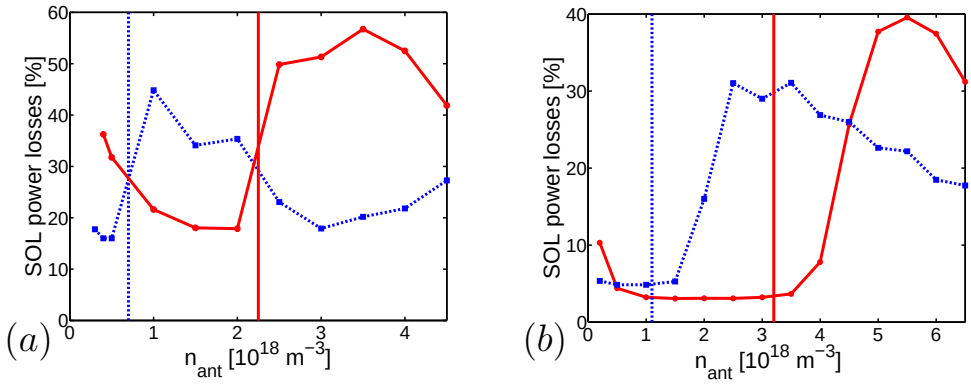

FIG. 4: Fraction of power lost to the SOL as a function of the density in front of the antenna for $n_\phi = -21$ (solid curve) and $n_\phi = -12$ (dashed curve), for an NSTX-U case with $B_T = 0.76$ T (fig. a) and $B_T = 1$ T (fig. b). The vertical lines represent the value of the density for which the FW cut-off starts to be "open" in front of the antenna.

2.0×10^{18} m^{-3}) together with the contour (in white) corresponding to the right hand cut-off in the cold plasma approximation. When the wave can propagate in the SOL the electric field outside of LCFS significantly increases.

In order to estimate the power lost to the SOL driven by a large electric field amplitude in the SOL, an artificial "collisional" damping mechanism has been implemented in AORSA as a proxy to represent the actual mechanism(s) which is(are) presently unknown [10, 11]. A collisional frequency, ν, has been implemented as the imaginary part of the angular frequency, ω, in the argument of the Plasma Dispersion function [10, 11].

The dashed curves in Figures 2(a) and 2(b) show the predicted absorbed power in the SOL region (SOL power losses) as a function of the density in front of the antenna ($n_{\rm ant}$) obtained by the 2D full wave code AORSA for a single (dominant) toroidal mode, $n_\phi = -21$ (Figure 2(a)) and -12 (Figures 2(b)) assuming $\nu/\omega = 0.01$. The cut-off of the fast wave corresponds to the right hand cut-off, which for a single ion species plasma and $\omega < |\omega_{\rm ce}|$, can be written as [3, 4]

$$n_{\rm e,FWcut-off} \propto \frac{k_\parallel^2 B}{\omega}, \tag{2}$$

where $k_\parallel$ and B are the parallel component of the wave vector and the equilibrium magnetic field, respectively. The vertical line in Figure 2 indicates when the wave is propagating in front of the antenna and the amplitude of the electric field starts to increase in the SOL region, as shown in Figure 1(b). Thus, a rapid transition in the fraction of the power lost to the SOL is found from the evanescent region to the propagating region both for $n_\phi = -12$ and -21. Moreover, for lower n_ϕ ($n_\phi/R = k_\phi \sim k_\parallel$) the transition occurs at lower $n_{\rm ant}$ as expected from Eq. 2.

In order to confirm this transition in terms of SOL power losses, 3D numerical simulations using 81 toroidal modes to reconstruct the full antenna spectrum have been

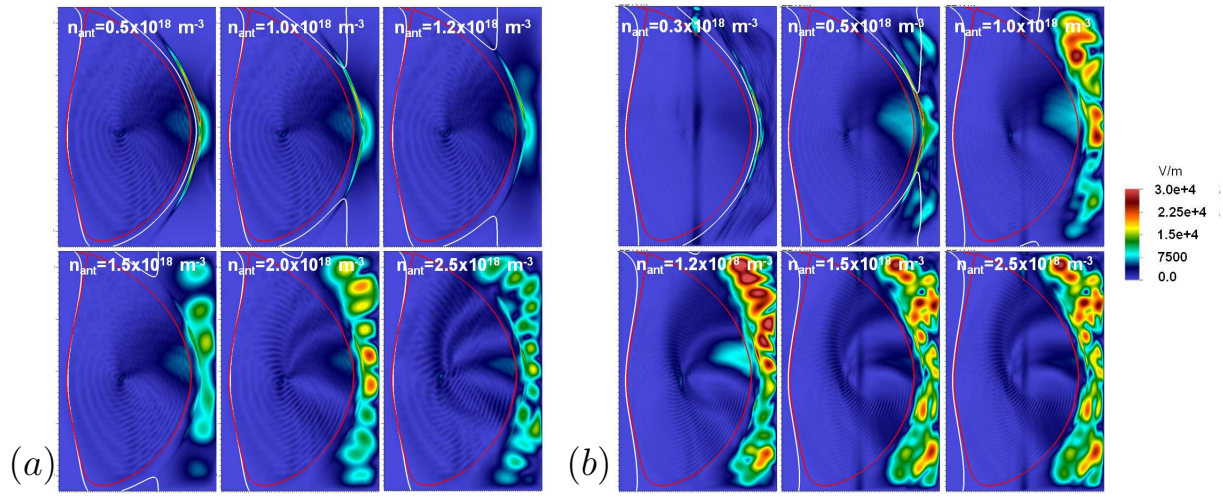

FIG. 5: Electric field amplitude for different density values in front of the antenna ($n_{\rm ant}$) (shown in the plots) with toroidal mode numbers $n_\phi = 15$ and $\omega/2\pi = 60$ MHz (a) and $\omega/2\pi = 90$ MHz (b), for DIII-D shot 111221. The white and red curves indicate the FW cut-off layer and the LCFS, respectively.

performed. Results are shown in Figures 2(a) and 2(b) by the solid curves. The 3D results exhibit similar behavior to that of the dominant mode (2D) runs and, in particular reproduce a similar transition in SOL power losses as a function of the density in front of the antenna, although it is less pronounced due to the contribution of the several toroidal modes. Larger SOL power losses in 3D runs with respect to the 2D runs are found for low and high $n_{\rm ant}$ and for both antenna phases. As a further confirmation of these results, we did the same 2D numerical analysis for another independent NSTX discharge, 130621, and the same edge loss transitions have been found (see Figure 2(c)) for both antenna phases.

Power deposition in the SOL has also been evaluated in 3D using 81 toroidal modes to reconstruct the full antenna spectrum for NSTX shot 130608 with $n_\phi = 21$ and $\nu/\omega = 0.01$. Figure 3 shows the 3D absorbed power deposition in the SOL for $n_{\rm ant} = 1.0 \times 10^{18}$ m^{-3} (Figures 3(a)-(c)), $n_{\rm ant} = 2.5 \times 10^{18}$ m^{-3} (Figures 3(d)-(f)) and three different ρ slices (ρ is the square root of the normalized poloidal flux): $\rho = 1.1$ to 1.15, near the antenna in figures 3(a) and 3(d), $\rho = 1.05$ to 1.1, the mid SOL in figures 3(b) and 3(e), $\rho = 1$ to 1.05, near the LCFS in figures 3(c) and 3(f) (the antenna is at $\rho = 1.15$). 3D SOL power losses are larger near the antenna (see figures 3(a) and 3(d)), and near the LCFS (see figure 3(c) and 3(f)), for low and high $n_{\rm ant}$ cases consistent with the experimental studies [7]. Moreover, for high $n_{\rm ant}$, large SOL power losses appear below the mid-plane due to the large RF field and they seem qualitatively to follow the magnetic field direction (the red curve in figure 3 represents a magnetic field line starting from the antenna and shows the large pitch angle of the magnetic field with respect to the antenna.)

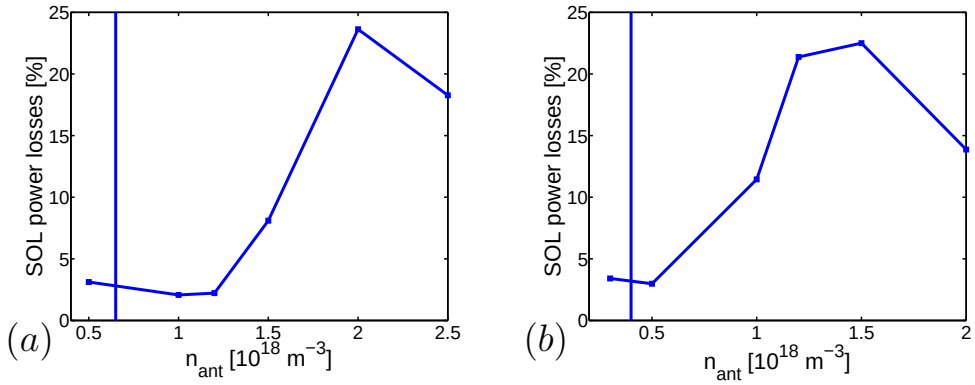

FIG. 6: Fraction of power lost to the SOL as a function of the density in front of the antenna for $\omega/2\pi = 60$ MHz (a) and $\omega/2\pi = 90$ MHz (b) with $n_\phi = 15$ for DIII-D shot 111221. The vertical lines represent the value of the density for which the FW cut-off starts to be "open" in front of the antenna (see Figs. 5a and 5a).

2.1 Predictions for NSTX-U

NSTX-U experiment will be operating at the beginning of 2015 [12] with a magnetic field (B_T) up to 1 T. Two H-mode scenarios for NSTX-U with $B_\mathrm{T} = 0.76$ T and $B_\mathrm{T} = 1$ T, obtained by using the TRANSP code [13], are here considered. Figure 4 shows the predicted RF power losses in the SOL as a function of n_ant for these NSTX-U cases with $B_\mathrm{T} = 0.76$ T (Figure 4(a)) and $B_\mathrm{T} = 1$ T (Figure 4(b)). The same strong transition to higher SOL power losses found in the NSTX case occurs for the NSTX-U case for both $n_\phi = -21$ (solid curve) and $n_\phi = -12$ (dashed curve) and for both magnetic field values. The main important difference with respect to the NSTX case is that the transition to higher losses in the SOL occurs at higher density as expected from Eq. 2 in which the FW cut-off is proportional to the magnetic field. Thus, with a higher magnetic field there will be a wider SOL density range in which the experiment can run with lower SOL power losses. This is a favorable condition for the HHFW performance in NSTX-U and it is in agreement with previous NSTX experimental observations [3].

3 Preliminary results on DIII-D and EAST devices

We extend our numerical simulations to "conventional" tokamaks with higher aspect ratios, such as DIII-D and EAST devices, in order to estimate the behavior of the RF power losses in "standard" geometry experiments and compare them with NSTX/NSTX-U results. Note that FW experiments in DIII-D are in the mid/high harmonic regime [14], while in EAST they are in the minority heating regime [15].

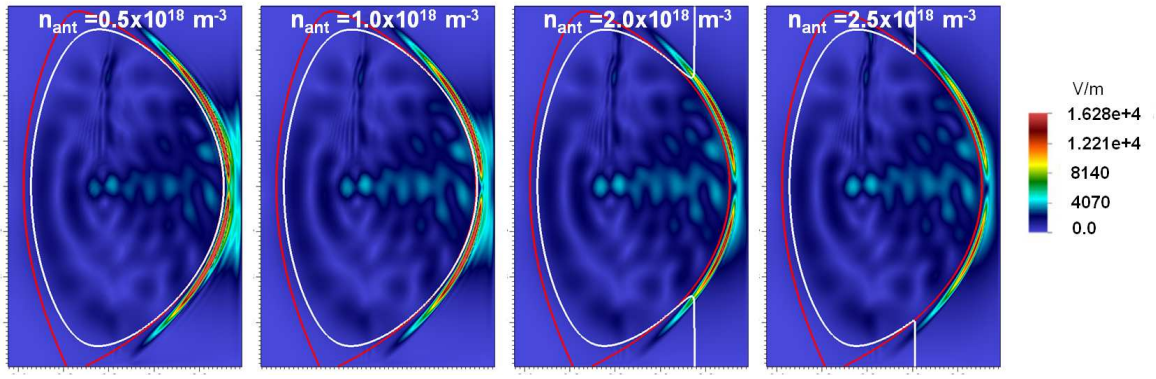

FIG. 7: Electric field amplitude for different density values in front of the antenna ($n_{\rm ant}$) (shown in the plots) with toroidal mode numbers $n_\phi = 12$ and $\omega/2\pi = 27$ MHZ, for EAST shot 36217. The white and red curves indicate the FW cut-off layer and the LCFS, respectively.

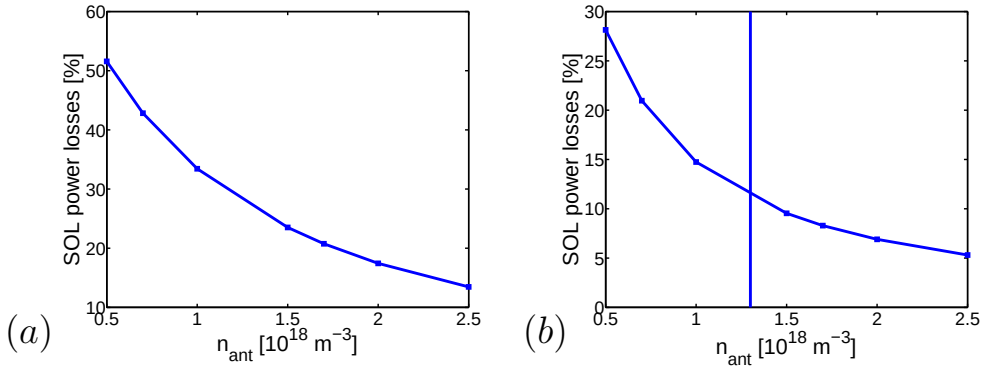

FIG. 8: Fraction of power lost to the SOL as a function of the density in front of the antenna with for $n_\phi = 23$ (a) and $n_\phi = 12$ (b) for EAST discharge 36217 . The vertical line in figure (a) represents the value of the density for which the FW cut-off starts to be "open" in front of the antenna.

3.1 DIII-D results

Previous work on DIII-D discussed the experimentally observed increase in edge losses as the SOL density increases in ELMy H-mode plasmas [16]. Figure 5 shows the electric field amplitude for DIII-D shot 111221 with $n_\phi = 15$ for $\omega/2\pi = 60$ MHz (Figure 5(a)) and $\omega/2\pi = 90$ MHz (Figure 5(b)). For both cases, the increasing of the electric field amplitude occurs when the wave can propagate outside the LCFS as found in NSTX and NSTX-U numerical analysis. The corresponding SOL power losses are shown in Figure 6 for both frequency values. We clearly see the same transition found in the results shown for NSTX/NSTX-U. In addition, for higher $\omega/2\pi$ the transition occurs at lower $n_{\rm ant}$ as expected from Eq. 2. This is a further confirmation of the validity of Eq.2 and the similarity with NSTX/NSTX-U results.

3.2 EAST results

As mentioned above, FW experiments in EAST operate in the minority heating regime, which differs from the mid/high harmonic regime adopted in DIII-D and NSTX. Figure 7 shows the electric field amplitude for EAST shot 36217 with $\omega/2\pi = 27$ MHz for $n_\phi = 12$ and different values of $n_{\rm ant}$ shown in the plots. Although the "standard" dominant toroidal mode in the EAST experiment is $n_\phi = 23$, we chose $n_\phi = 12$ in order to study the beahvior of the SOL power losses with and without an evanescent layer in front of the antenna for this specific EAST shot as done for NSTX/NSTX-U and DIII-D cases. In Figure 7, one can note that, unlike NSTX/NSTX-U and DIII-D, the electric field amplitude does not increase outside of LCFS with increasing $n_{\rm ant}$, even when the wave can propagate in the SOL. Only a significant parallel component of the electric field is found in the SOL and is apparently larger than NSTX cases. Figure 8 shows the SOL power losses as a function of $n_{\rm ant}$ with $n_\phi = 23$ (Figure 8(a)) and $n_\phi = 12$ (Figure 8(b)). Unlike Figure 8(b), note that in Figure 8(a) the wave is always evanescent in the SOL for the given density range. The behavior of the SOL power losses shown in Figure 8 disagrees with the behavior shown in Figures 2, 4, and 6; in other words, in the EAST numerical analysis the transition to higher SOL power losses does not appear. Further studies are needed in order to fully understand the differences between NSTX/NSTX-U/DIII-D and EAST results. Moreover, implementation of a more realistic boundary condition (limiter boundary) in the full wave code AORSA is underway with the aim of better understanding the behavior of the standing wave outside of the LCFS.

Acknowledgments. This material is based upon work supported by the U.S. Department of Energy, Office of Science, Office of Fusion Energy Sciences under contract numbers DE-FC02-01ER54648, DE-AC02-09CH11466, and DE-AC02-05CH11231.

References

[1] GORMEZANO, C., et al., Nucl. Fusion **47**, S285S336 (2007).
[2] ONO, M., et al., Nucl. Fusion **40**, 557 (2000).
[3] HOSEA, J. C., et al., Phys. Plasmas **15**, 056104 (2008).
[4] PHILLIPS, C. K., et al., Nucl. Fusion **49**, 075015 (2009).
[5] TAYLOR, G., et al., Phys. Plasmas **17**, 056114 (2010).
[6] PERKINS, R. J., et al., Phys. Rev. Lett. **109**, 045001 (2012).
[7] PERKINS, R. J., et al., Nucl. Fusion **53**, 083025 (2013).
[8] JAEGER, E. F., et al., Phys. Plasmas **8**, 1573 (2001).
[9] GREEN, D. L., et al., Phys. Rev. Lett. **107**, 145001 (2011).
[10] BERTELLI, N., et al., AIP Conf. Proc. **1580**, 310 (2014).
[11] BERTELLI, N., et al., Nucl. Fusion **54**, 083004 (2014).
[12] MENARD, J.E., et al., Nucl. Fusion **52**, 083015 (2012).
[13] GERHARDT,S.P., et al., Nucl. Fusion **52**, 083020 (2012).
[14] PINSKER, R. I., et al., Nucl. Fusion **46**, S416 (2006).
[15] ZHANG, X.J., et al., Nucl. Fusion **53**, 023004 (2013).
[16] PETTY, C. C., et al., Nucl. Fusion **39**, 1421 (1999).